Correlation of Characteristic Ne SXR Signal Pulse With Computed Plasma Focus Dynamics in the Ne (97.5%)–Kr (2.5%) Admixtures of the INTI PF Machine at 12 kV

Federico Apilado Roy Jr., *Member, IEEE*, Sor Heoh Saw, Paul Choon Keat Lee, Rajdeep Singh Rawat, and Sing Lee

***Abstract*— This paper shows the correlation of the characteristic Ne soft X-ray (SXR) signal pulse with computed dynamics of the plasma focus using doped neon in Ne (97.5%)/Kr (2.5%) admixtures. The Lee model code is coupled with a specifically designed correlation excel template. The results show that typically, the characteristic Ne SXR pulse signal starts after the start of the reflected shock (RS) and before the beginning of the pinch. Specifically, in the illustrated shot, the RS phase starts at 3.375 μs while the pinch phase starts at 3.384 μs. The characteristic Ne SXR signal pulse starts at 3.377 μs, which is 2 ns after the start of the RS and 7 ns before the pinch starts. There is a consistent trend of Ne SXR correlation with the computed dynamics in the Ne doped with Kr admixtures up to a doping level of 2.5%.**

***Index Terms*— Characteristic Ne soft X-ray (Ne SXR) signal pulse, INTI plasma focus (PF), Lee model code, Ne SXR yield, pinch phase, reflected shock (RS) phase.**

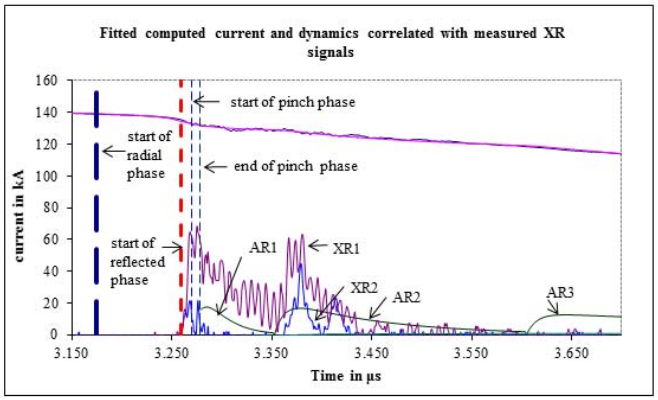

Fig. 1. Correlating the measured Ne SXR pulse (difference pulse of XR1 − XR2) with the fitted computed and measured current traces. The fitting is good and the current traces overlap (top trace).

I. Introduction

THE dense plasma focus (DPF) [1] produces copious Ne soft X-ray (SXR) [2]–[20]. DPF devices are classified into type-T1 and type-T2 [19], with low static inductance L_0 (tens of nanohenries) and high L_0 (>100 nH), respectively.

The INTI DPF is type-T2 with $L_0 = 110$ nH [4], requiring the Lee code [20] in the six-phase version for fitting the computed current wave shape to the measured waveform.

When such a fitting is done, the code outputs the dynamics of the axial and radial phases of the plasma focus (PF) waveforms and also the times of the Ne SXR pulse (characteristic He-like and H-like) relative to the plasma dynamics. This had been done for INTI PF for the case of operation in pure neon [4], [6]. We now proceed to do this correlation for the operation of neon doped with krypton (see Fig. 1).

Fig. 1 shows the measured and fitted computed currents and the time comparison of the detected Ne SXR pulses with the computed dynamics. The Ne SXR pulse is the pulse that the results from a subtraction of XR2 from XR1. The dashed vertical lines represent the time positions of the beginnings of radial phase, reflected shock (RS), and the pinch phase, also when the pinch terminates. The three anomalous resistances (ARs) (AR1, AR2, and AR3) phases are also indicated.

On the other hand, the previous work deals with operation in pure neon without reference to RS phase; this work deals with operation in krypton-doped neon and extends the correlation to include the time position of RS as well.

II. Lee Model Code

Our code interacts the circuit equations with the equations of motion taking into account thermodynamics and radiation. The resultant simulation is found to be realistic for actual usage in PFs such as United Nations University/International Centre for Theoretical Physics PF Facility [21]–[25], NX1 [11], [26], and NX2 [23], [26], [27]. The code has been modified for

Manuscript received March 30, 2016; revised July 9, 2016, February 4, 2017, and December 5, 2018; accepted December 28, 2018. Date of current version February 11, 2019. The review of this paper was arranged by Senior Editor S. J. Gitomer. *(Corresponding author: Sor Heoh Saw.)*

F. A. Roy Jr. is with the Centre for Plasma Research, INTI International University, Nilai 71800, Malaysia (e-mail: fedroy2003@yahoo.com).

S. H. Saw is with the Plasma Research Group, Centre for Research Excellence, Nilai University, Nilai 71800, Malaysia, and also with the Institute for Plasma Focus Studies, IPFS, Melbourne, VIC 3148, Australia (e-mail: saw.ipfs@gmail.com).

P. C. K. Lee and R. S. Rawat are with the National Institute of Education, Nanyang Technological University, Singapore 637616 (e-mail: paul.lee@nie.edu.sg; rajdeep.rawat@nie.edu.sg).

S. Lee is with IPFS, Melbourne, VIC 3148, Australia, with INTI International University, Nilai 71800, Malaysia, and also with the Department of Physics, University of Malaya, Kuala Lumpur 50603, Malaysia.

Color versions of one or more of the figures in this paper are available online at http://ieeexplore.ieee.org.

Digital Object Identifier 10.1109/TPS.2019.2891556

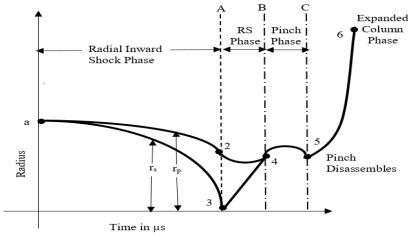

Fig. 2. Radial dynamics. Vertical line A: start of the RS phase. Vertical line B: end RS phase/beginning of pinch. Vertical line C: pinch phase ends.

DENA [28], a Filippov-type DPF. The code has been used to derive Ne SXR scaling laws [7]. A template was developed to reduce the work in correlating the time positions of the detected SXR pulses with the PF dynamics [19].

The PF dynamics is computed in two main phases, the axial followed by the radial.

The radial phase is further computed as subphases (Fig. 2): the inward shock (lines denoted by a-2 and a-3), the RS (2–4 and 3–4), the pinch, or slow compression [4 and 5 followed by the expanded column (lines 5 and 6)]. The plasma slug starts to be formed (point a). The piston (magnetic) radius r_p and the inward shock radius r_s decreases until $r_s = 0$ (point 3), then the RS phase, and then the pinch phase (curves 4 and 5). The pinch breakup is simulated as a sudden expansion (curves 5 and 6) [29]–[31].

The focus pinch produces energetic particles and radiation including SXRs. The breakup of the pinch resulting in a low-density large column is postulated to occur abruptly with disruptions and randomly distributed small regions of extreme conditions. These effects are simulated only in the gross sense, outputting only average temperature and density.

Our simulation uses four fitting parameters f_m and f_c (mass and current fractions for axial dynamics) and radial phase equivalents f_{mr} and f_{cr} in the fitting process. These model parameters represent the nett effects of mass, energy, and charge balances accounting for all processes including those processes which are not specifically simulated. The output features including trajectories and velocities, and SXR yields in various machines are found to be consistent with observed values [3], [4], [6].

In the simulation [19], Q_L, the quantity of line radiation, is expressed in SI units by the following equation:

$$\frac{dQ_L}{dt} = -4.6 \times 10^{-31} {n_i}^2 Z {Z_n}^4 \left(\pi r_p^2\right) z_f / T \qquad (1)$$

Here, Q_L is the line radiation. However, the conditions of our experiment are chosen so that the pinch temperatures are in the range of 1–6 $\times$ 10^6 K so that the Ne plasma is predominantly eighth and ninth ionized; so that the line radiation is predominantly H-like and He-like, and we may that we take Q_L to be the characteristic Ne SXR yield. In our code, the Ne SXR quantity is integrated for the pinch duration. Thus, the Ne SXR energy produced in the pinch depends on: ion density n_i, effective charge Z, pinch radius r_p, pinch length z_l, temperature T, and lifetime of the pinch. Here, Z_n is the atomic number.

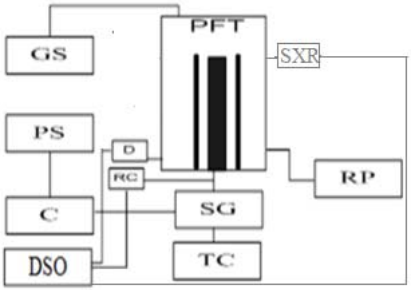

Fig. 3. Block diagram of INTI PF. PFT = PF assembly, GS denotes the supply of gas, PS is the power supply, *C* is the capacitor, SG is the spark gap, TC is the triggering unit, RP is the rotary pump, *D* is the voltage divider, *RC* is the *dI/dt* coil, and SXR denotes the DXS spectrometer [19].

This produced energy is attenuated by self-absorption before emission. The code computes and accounts for this volumetric self-absorption. It turns out that within the parameters of the experiments for this paper, the self-absorption effects are not significant. Moreover, for fully ionized plasma, radiation is mainly bremsstrahlung when temperature is too high. On the other hand, the Ne plasma needs sufficient temperature to reach the He-like and H-like ionization. Lee *et al.* [7] proposed that $T = 3 \times 10^6$ K is optimum. Bing's [32] work and further simulation indicated that for our code, a range of 1.5–2 $\times$ 10^6 K is needed for the optimum emission of the characteristic Ne SXR. To account for these effects, the code implements a T window, within which the computed Q_L is taken as characteristic Ne SXR.

III. Experimental Setup and Methodology

Fig. 3 shows a schematic of the setup. We operate at 12 kV using Ne–Kr admixtures. The Ne SXR pulses are recorded using two channels of the diode x-ray spectrometer (DXS). The current–time *dI/dt* and the voltage across the electrodes are also recorded on a digital storage oscilloscope (four channels) with 1-GSa/s sample rate. A resistive divider with 15-ns response was used for the voltage (V) measurement [21]. A coil with seven turns wrapped around one of the 16 return conductors was used to measure the *dI/dt* signal [33].

The two Ne SXR detectors of DXS [34]–[36] are used in a filtered configuration, denoted by Ch1 and Ch2, to measure SXR by subtraction [19]. Each channel uses a fast, wide-range photodiode (BXP65 with window removed). Ch1 is filtered by 13-μm aluminum foil while Ch2 is filtered by 125-μm mylar film with addition of 3-μm aluminum foil.

Fig. 4 shows the spectral sensitivity of Ch1 and Ch2. The two sensitivity curves are designed to identically overlap in the spectral range from 0 to 20 keV, except for the additional spiked feature within 900–1550 eV. This feature belongs to Ch1 only. This range of 900–1550 eV is the spectral range of the characteristic He-like, H-like SXR emission from neon. Subtracting Ch2 from Ch1 [37] enables the computation of the quantity of characteristic Ne SXR. If there is a difference, it can only come from radiation within the 900–1550-eV spectral range which is from Ne SXR. Furthermore, if identical pulses are measured by Ch1 and Ch2, hence, with no difference in the signals, then the channels are measuring radiation above 1550 eV, which is more energetic radiation.

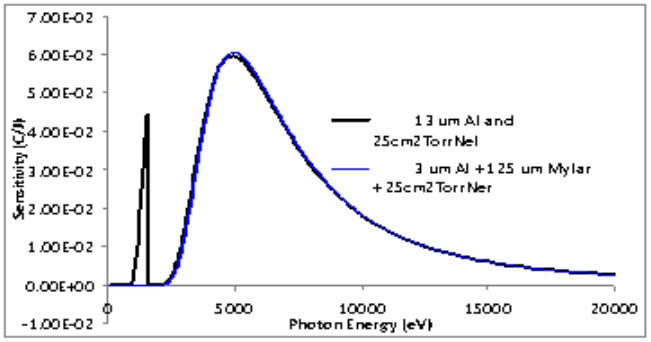

Fig. 4. Two Ch1 and Ch2 channels have the identical sensitivity curves for the spectral range from 1550 eV to 20 keV and beyond. Ch1 has an additional feature sensitivity spike from 900 to 1550 eV not shared with Ch2.

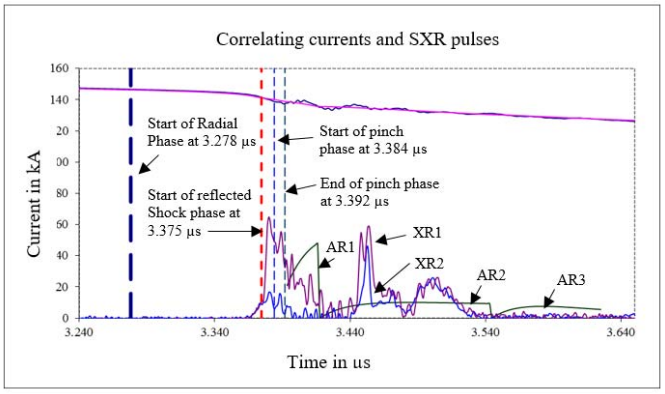

Fig. 5. Correlating the measured characteristic He-like and H-like Ne SXR pulses with the PF dynamics of S14.

Both detectors are normalized to one another at the same distance to the pinch position. In this way, dI/dt, V, and SXR pulse are measured. These measured quantities are then correlated with the simulated current and radial trajectories, computed with the code with the fitted current forming a firm connection between the code and the reality of the experiment.

For presentation in this paper, investigations on Ne SXR yield from neon doped with krypton were carried out to determine the comparison of the characteristic Ne SXR pulses with the radial dynamics. The standard anode dimensions ("a" = 0.95 cm and z_0 = 16 cm) of the INTI PF machine were used.

Seventeen shots were fired at 12-kV, 2.0-torr normal conditioning procedures.

The ratio of the Ne–Kr admixtures is Ne (97.5%) + Kr (2.5%). We illustrate the method which we use to fill the system with the mixture with the procedure for the following example. For the mixture of Ne (97.5%) + Kr (2.5%), we pump the chamber down to low (base of less than 0.01 torr) pressure, fill with Ne up to 2.0 torr, then pump down to 1.95 torr and let in Kr until the pressure is 2.0 torr. In effect, the pressure of Kr in the mixture is 0.05 torr giving the mixture of Ne (97.5%) and Kr (2.5%). To run the code for this mixture, we assume that the thermodynamic properties of the mixture are the same as Ne (since the mixture is predominantly Ne). However, the small percentage of Kr has a disproportionately large mass loading effect due to the atomic weight of Kr being 84 compared to Ne of 20. In other words, 1% of Kr in the mixture contributes more than 4% to the inertia of the gas being driven by the current sheet. Hence, we need to obtain the equivalent loading (in terms of operating pressure) to input into the code. For a 2.0-torr mixture, the equivalent Ne pressure to input into the Lee code is

$$P_0 = 2[(\%\mathrm{Ne} + \{84/20\}\%\mathrm{Kr})/100]. \tag{2}$$

We need to state at this point that this "equivalent pressure" method merely provides the extra mass loading that doping with Kr would result in. We estimate that it would give the correct axial phase dynamics (in the manner we model) and very nearly the correct radial dynamics. This gives us a simple method to model the dynamics of the Kr-doped PF so that we can compare the time profile of the measured Ne SXR yield against computed dynamics at least to a first order of approximation.

The following sections will discuss the observations made on the characteristic Ne SXR yields of the Ne (97.5%)–Kr (2.5%) admixtures. It includes the Ne SXR yield for a particular shot S14, the characteristics of the Ne SXR yield, and its correlation to the fitted current trace and to the computed PF dynamics. It analyzes the correlation of the Ne SXR yield in the Ne–Kr admixtures of this particular shot. The Ne SXR signal is correlated with the beginning of the RS and the beginning of the pinch.

IV. Results

The results are shown in Fig. 5 and discussed. The set of lines is time markers to help visualize the correlation of measured characteristic Ne SXR with the computed RS and pinch phases. For detailed comparison, the SXR pulses are aligned at the start of the radial dynamics [vertical left lines shown in Fig. 5 (left)]. In Fig. 5, the first SXR pulse is seen to start and increases in amplitude during the time between the RS and start of the pinch phase. This pulse is predominantly Ne SXR (noting that the difference on the pulses). It decreases until the end of the first AR1. It again increases with lower amplitude at the start of the second AR2 and decreases until the middle of the second AR. Finally, the last pulse is an SXR which is harder than the characteristic Ne SXR lines. This is evident from the identical signals of Ch1 and Ch2 over the duration of this last pulse. The harder SXR lasts until before the end of the second AR. There is no SXR signal detected in the AR3 period.

The results for this shot show that the Ne SXR pulse starts sharply at 3.377 μs which is 2 ns after the beginning of RS at 3.375 μs and 7 ns before the beginning of the pinch phase at 3.384 μs; the pulse drops in magnitude through the duration of the pinch phase (8 ns) and continues to drop toward 0 for another 32 ns that coincides with the end of the first AR1. At the end of the first AR, another pulse of lower amplitude starts to increase with significantly lower characteristic Ne SXR yield (due to the smaller difference between channel 1 and channel 2). This second characteristic Ne pulse lasts for duration of 54 ns. Finally, toward the middle of the second AR, an X-ray (XR) pulse is emitted. This pulse is harder than

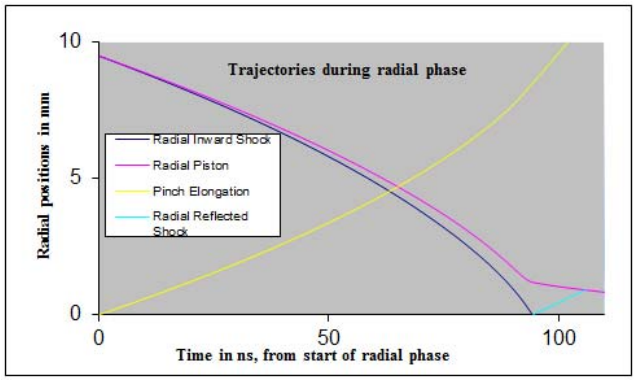

Fig. 6. Trajectories during the radial phase.

the characteristic Ne SXR lines, and lasts for 62 ns until the end of the second AR2. There is no signal detected at the third AR3. The Ne SXR yield for this example is 4.5 J.

Study of these shots at 12 kV at 2.2 torr (equivalent Ne pressure) establishes that this correlation is typical. The Ne SXR line yields lie in the range of 0.8–4.5 J. The shots with the higher yields have larger pulsewidths, some with significant contributions from the AR regimes. This range of yields compares with [4] and [6] in the same PF with pure Ne at 2 torr, yielding consistently a range of 1–2 J with occasional shots at 3–4 J, averaging 2 J over a large number of shots. From the data, the Kr-doped shots appear to have a more variable yield from shot-to-shot than the shots with pure Ne.

For the shot (S14) portrayed in Fig. 5, the minimum radius $r_{\min}$ computed by the code, configured for this shot by fitting computed to measured current waveforms, is 0.77 mm (see Fig 6) giving a radius ratio $r_{\min}/a = 0.081$ (minimum value). Peak inward shock speed is 24.8 cm/μs and peak inward piston speed reached 15.5 cm/μs. The peak inward shock speed corresponds to a temperature of 2.8×10^6 K as inward shock goes on axis. This temperature is within the characteristic Ne SXR emission window; however, the ion density is low. RS would double this temp to 5.6×10^6 K as it starts to come off axis. (This temperature is still within the characteristic Ne SXR emission window.) As RS moves outwards from the axis, the initial volume of this higher density region is small but increases rapidly as RS moves outwards toward piston, hitting the piston at a radial distance of 0.92 mm. This marks the beginning of the pinch; the piston further compressing the pinch until the minimum radius of 0.77 mm. Piston-shock wave system imparts 60 J to the radial system up to the end of the pinch. Following the pinch breakup, anomalous resistive heating is 20 J per 10 ns supported 1 kJ of energy stored in the external inductance and inductance formed by the plasma current at end of pinch.

V. Conclusion

The SXR pulses from INTI PF at 12 kV for the Ne (97.5%)/Kr (2.5%) admixtures at an equivalent pressure of 2.2-torr Ne are differentiated into Ne SXR (spectral range of 900–1550 eV) and other (noncharacteristic) Ne SXR emission with spectral energy $>$ 1550 eV. These SXR pulses are correlated with the computed currents fit to the measured to maintain the connection between the simulation of the code and the reality of the measured quantities. It is found typically that the characteristic Ne SXR pulse starts sharply between the RS phase starting time and the pinch starting time, achieving peak amplitude during these 9 ns, dropping to 0 through the first AR1 AR phase. During the next AR period, arises a second XR pulse which consists of mainly noncharacteristic Ne SXR and which lasts for 54 ns. Finally, a harder XR than the characteristic Ne SXR lines occurs for 62 ns.

In brief, the characteristic He-like and H-like Ne line SXR pulses begins sharply coinciding in time to a time after the start of the RS phase. There is a strong emission of Ne SXR before the pinch phase, during the pinch phase with the emission tailing off after the pinch phase. After this Ne SXR pulse, several harder XR pulses are emitted which consist of noncharacteristic Ne XR, likely to be bremsstrahlung.

We compare the differences between pure Ne- and Kr-doped Ne. The measurements for pure Ne have been presented in detail in [4] and [6]. For pure Ne, the profile is very distinct with abrupt (almost vertical) emission of Ne SXR and lasting 30–50 ns on the average and distinct differences in magnitude of signals of both channels. For Ne (97.5%)/Kr (2.5%) admixtures at an equivalent pressure of 2.2-torr Ne, however, in contrast to the sharp rise, there is a small hump (sometime a separate hump) before the start of RS (around 3–7 ns) (see Fig 5). The pre-RS hump with both channels inseparably together grows progressively bigger for 5% Kr and 10% Kr. The evidence taken together indicates that this small hump is due primarily to Kr radiation in the RS column just before RS hits the piston. Examining the postpinch pulses which are labeled AR1, AR2, and AR3, and comparing with the typical case for pure Ne, there is evidence that the Kr-doped case has bigger pulses. The evidence is that this region is contributed to the Kr emission in the Kr-doped shots. The code computes the characteristic neon yield by means of (1) with the implementation of a suitable temperature window within which the Ne plasma reaches its H-like and He-like ionization states. The code does include bremsstrahlung during the pinch phase but not after the pinch phase and also does not include Kr radiation for the Kr doped cases. It would be of interest to obtain time-resolved images correlated with the XR pulses to further substantiate the above discussion which, for the moment, depends on the mechanisms built into the code.

The results of this paper have implications in improving the model code for a more comprehensive computation not only just for the characteristic He-like and H-like Ne line SXR yields but also to include the harder radiation from bremsstrahlung.

References

[1] J. W. Mather, "Formation of a high-density deuterium plasma focus," *Phys. Fluids*, vol. 8, no. 2, p. 366, 1965, doi: 10.1063/1.1761231.

[2] S. H. Saw, P. C. K. Lee, R. S. Rawat, and S. Lee, "Optimizing UNU/ICTP PFF plasma focus for neon soft X-ray operation," *IEEE Trans. Plasma Sci.*, vol. 37, no. 7, pp. 1276–1282, Jul. 2009, doi: 10.1109/TPS.2009.2022167.

[3] S. Lee, R. S. Rawat, P. Lee, and S. H. Saw, "Soft X-ray yield from NX2 plasma focus," *J. Appl. Phys.*, vol. 106, no. 2, p. 023309, 2009, doi: 10.1063/1.3176489.

[4] S. Lee *et al.*, "Correlation of measured soft X-ray pulses with modeled dynamics of the plasma focus," *IEEE Trans. Plasma Sci.*, vol. 39, no. 11, pp. 3196–3202, Nov. 2011, doi: 10.1109/TPS.2011.2166812.
[5] M. Liu, X. Feng, S. V. Springham, and S. Lee, "Soft X-ray yield measurement in a small plasma focus operated in neon," *IEEE Trans. Plasma Sci.*, vol. 26, no. 2, pp. 135–140, Apr. 1998.
[6] S. H. Saw *et al.*, "SXR measurements in INTI PF operated in neon to identify typical (normal N) profile for shots with good yield," *IEEE Trans. Plasma Sci.*, vol. 41, no. 11, pp. 3166–3172, Nov. 2013, doi: 10.1109/TPS.2013.2281333.
[7] S. Lee, S. H. Saw, P. Lee, and R. S. Rawat, "Numerical experiments on plasma focus neon soft X-ray scaling," *Plasma Phys. Control. Fusion*, vol. 51, no. 10, p. 105013, 2009, doi: 10.1088/0741-3335/51/10/105013.
[8] S. Al-Hawat, M. Akel, S. Lee, and S. H. Saw, "Model parameters versus gas pressure in two different plasma focus devices operated in argon and neon," *J. Fusion Energy*, vol. 31, no. 1, pp. 13–20, 2012, doi: 10.1007/s10894011-9414-3.
[9] A. Serban and S. Lee, "Experiments on speed-enhanced neutron yield from a small plasma focus," *J. Plasma Phys.*, vol. 60, no. 1, pp. 3–15, Aug. 1998, doi: 10.1017/S0022377898006771.
[10] M. A. Mohammadi, S. Sobhanian, C. S. Wong, P. Lee, and R. S. Rawat, "The effect of anode shape on neon soft X-ray emissions and current sheath configuration in plasma focus device," *J. Phys. D: Appl. Phys.*, vol. 42, no. 4, p. 045203, 2009.
[11] S. Lee *et al.*, "High rep rate high performance plasma focus as a powerful radiation source," *IEEE Trans. Plasma Sci.*, vol. 26, no. 4, pp. 1119–1126, Aug. 1998, doi: 10.1109/27.725141.
[12] Y. Kato and S. H. Be, "Generation of soft x rays using a rare gas-hydrogen plasma focus and its application to X-ray lithography," *Appl. Phys. Lett.*, vol. 48, no. 11, p. 686, 1986, doi: 10.1063/1.96743.
[13] S. Al-Hawat, M. Akel, and S. Lee, "Numerical experiments on Neon soft X-ray optimization of AECS-PF2 plasma focus device," *J. Fusion Energy*, vol. 30, no. 6, pp. 494–502, Dec. 2011, doi: 10.1007/s10894-011-9416-1.
[14] A. E. Abdou, M. I. Ismail, A. E. Mohamed, S. Lee, S. H. Saw, and R. Verma, "Preliminary results of Kansas State University dense plasma focus," *IEEE Trans. Plasma Sci.*, vol. 40, no. 10, pp. 2741–2744, Oct. 2012, doi: 10.1109/TPS.2012.2209682.
[15] S. Zapryanov, V. Yordanov, and A. Blagoev, "Measurements of the basic characteristics of the dense plasma focus device," *Bulg. J. Phys.*, vol. 38, no. 2, pp. 184–190, 2011.
[16] M. Mathuthu, T. G. Zengeni, and A. V. Gholap, "Measurement of magnetic field and velocity profiles in 3.6 kJ United Nations University/international center for theoretical physics plasma focus fusion device," *Phys. Plasmas*, vol. 3, no. 12, p. 4572, 1996, doi: 10.1063/1.871583.
[17] H. krompholz, F. Rühl, W. Schneider, K. Schönbach, and G. Herziger, "A scaling law for plasma focus devices," *Phys. Lett A*, vol. 82, no. 2, pp. 82–84, Mar. 1981, doi: 10.1016/0375-9601(81)90944-0.
[18] Y. H. Chen and S. Lee, "Coaxial plasma gun in mode 1 operation," *Int. J. Electron.*, vol. 35, no. 3, pp. 341–352, 1973.
[19] S. Lee, S. H. Saw, A. E. Abdou, and H. Torreblanca, "Characterizing plasma focus devices—Role of the static inductance—Instability phase fitted by anomalous resistances," *J. Fusion Energy*, vol. 30, no. 4, pp. 277–282, Aug. 2011, doi: 10.1007/s10894-010-9372-1.
[20] S. Lee, "Plasma focus radiative model: Review of the Lee model code," *J. Fusion Energy*, vol. 33, no. 4, pp. 319–335, Aug. 2014, doi: 10.1007/s10894-014-9683-8.
[21] S. Lee *et al.*, "A simple facility for the teaching of plasma dynamics and plasma nuclear fusion," *Amer. J. Phys*, vol. 56, no. 1, pp. 62–68, 1998, doi: 10.1119/1.15433.
[22] M. Liu, "Soft X-rays from compact plasma focus," Ph.D. dissertation, School Sci., NIE, Singapore, 1996.
[23] S. Lee and A. Serban, "Dimensions and lifetime of the plasma focus pinch," *IEEE Trans. Plasma Sci.*, vol. 24, no. 3, pp. 1101–1105, Jun. 1996, doi: 10.1109/27.533118.
[24] S. Lee, "In twelve years of UNU/ICTP PFF-A review," Abdus Salam ICTP, Trieste, Italy, pp. 5–34, Tech. Rep. IC/98/231, 1998, pp. 5–34.
[25] S. V. Springham, S. Lee, and M. S. Rafique, "Correlated deuteron energy spectra and neutron yield for a 3 kJ plasma focus," *Plasma Phys. Controlled Fusion*, vol. 42, no. 10, pp. 1023–1032, 2000, doi: 10.1088/0741-3335/42/10/302.
[26] G. Zhang, "Plasma soft X-ray source for microelectronic lithography," Ph.D. dissertation, School Sci., NIE, Nanyang Technological Univ., Singapore, 1999.
[27] D. Wong *et al.*, "An improved radiative plasma focus model calibrated for neon-filled NX2 using a tapered anode," *Plasma Sources Sci. Technol.*, vol. 16, no. 1, pp. 116–123, 2007, doi: 10.1088/0963-0252/16/1/016.
[28] V. Siahpoush, M. A. Tafreshi, S. Sobhanian, and S. Khorram, "Adaptation of Sing Lee's model to the Filippov type plasma focus geometry," *Plasma Phys. Control. Fusion*, vol. 47, no. 7, p. 1065, 2005, doi: 10.1088/0741-3335/47/7/007.
[29] F. A. Roy, Jr., "Investigation and optimization of neon soft X-ray of the INTI plasma focus at 12 kV," Centre Plasma Res., INTI Int. Univ., Nilai, Malaysia, 2016.
[30] S. Lee. (2007). *Radiative Dense Plasma Focus Computation Package: RADPF*. [Online]. Available: http://www.plasmafocus.net/IPFS/modelpackage/File1RADPF.htm
[31] S. Lee and S. H. Saw, "The plasma focus-numerical experiments, insights and applications," in *Plasma Science and Technology for Emerging Economies*, R. S. Rawat, Ed. Singapore: Springer, 2017, doi: 10.1007/978-981-10-4217-1_3.
[32] S. Bing, "Plasma dynamics and X-ray emission of the plasma focus," Ph.D. dissertation, School Sci., NIE, Nanyang Technological Univ., Singapore, 2000.
[33] S. H. Saw *et al.*, "*In situ* determination of the static inductance and resistance of a plasma focus capacitor bank," *Rev. Sci. Instrum.*, vol. 81, p. 053505, May 2010, doi: 10.1063/1.3429207.
[34] A. G. Michette and C. J. Buckley, *X-Ray Science and Technology*. Bristol, U.K.: Institute of Physics Publishing, 1993, p. 249.
[35] B. L. Henke, E. M. Gullikson, and J. C. Davis, "X-Ray interactions: Photoabsorption, scattering, transmission, and reflection at E= 50-30,000 eV, Z= 1-92," *At. Data Nucl. Data Tables*, vol. 54, no. 2, pp. 181–342, Jul. 1993.
[36] E. Kroupp *et al.*, "Investigation of Ne IX and Ne X line emission from dense plasma using Ross-filter systems," *J. Appl. Phys.*, vol. 92, no. 9, pp. 4947–4951, Nov. 2002, doi: 10.1063/1.1512316.
[37] S. H. Saw *et al.*, "Magnetic probe measurements in INTI plasma focus to determine dependence of axial speed with pressure in neon," *J. Fusion Energy*, vol. 31, no. 5, pp. 411–417, Oct. 2012, doi: 10.1007/s10894-011-9487-z.

Authors' photographs and biographies not available at the time of publication.